A novel model based-design approach for a dynamic positioning system

M. Martelli*, N. Faggioni* & S. Donnarumma*

**Dept. of Electrical, Electronic, Telecommunications, Naval Architecture and Marine Engineering (DITEN), Polytechnic School of Genoa University, Genova, Italy.*
* Corresponding Author. Email: michele.martelli@unige.it

Synopsis

This paper aims to present a novel approach to design a dynamic positioning system by using a dynamic model based-design approach. The proposed study has been performed to both develop and preliminarily test the control logic that should be implemented on a model scale vessel. Indeed, the proposed tool has been designed for a fully actuated tug vessel equipped with two azimuthal thrusters and one bow-thruster, emulated in behaviour with a dynamic simulator. Thanks to the model actuation, it was possible to design a unique, optimised allocation logic able to fulfil both open-loop and closed-loop commands, sufficiently proved and tuned before the installation onboard. Moreover, a thorough comparison between different design methods, static and dynamic performance evaluation has been carried out. Two different operational modes are tested, and the results are presented: joystick and station keeping.

Keywords: Dynamic Positioning, Control Optimisation, Model-based Analysis, Motion Control

1. Introduction

Since the early 1970s, Dynamic Positioning (DP) has been of significant interest for the oil industry, e.g. by Balchen et al. (1976). Indeed, from its first applications, DP has proved to be a fundamental tool for equipping ships able to work in the offshore environment. Over the last few years, as it happens for all the technologies, DP has found its applications in different marine fields and the studies carried out for station keeping have been generalised to the low-speed motions control which is crucial for the autonomous navigation.

The design of dynamic positioning systems is a complex subject based on the automatic control of ship motions. For such a reason, it requires the integration of several sub-systems and their mutual interactions. In this context, the controller is the kernel of the DP. Model-based design research regarding DP controller design has been discussed in Sørensen et al. (1996) and Donnarumma et al. (2015-2017). In the present work, the DP controller designed for a case study is based on the Lagrange multiplier technique, e.g. Johansen et al. (2013). The preliminary assessment of DP performance is the first step for the propulsion system design in terms of sizing and configuration. The initial analysis of the station-keeping capability is carried out via static approaches, (Reilly et al., 2011), and (Xu at al., 2015). In this context, dynamic positioning capability polar plots (DPCPs) have become standard tools for the design and management of DP systems. The standard procedure to evaluate the DPCP is by using a static equilibrium; however, this will not represent the real system capabilities due to the several dynamics involved in the process. Wang et al. (2018) show the importance of adequately modelling environmental disturbances in order to assess as feasible dynamic performance as possible employing static analysis. This work aims to use a dynamic simulation platform to both validate and optimise the allocation logic; and to evaluate the system performance by means of time-domain simulations. For this purpose, a custom dynamic simulator of a case study vessel has been developed. Such a case study refers to a fully actuated tug model, equipped with two azimuthal thrusters and one bow-thruster, where a dynamic positioning system, together with necessary sensors and controllers, has been designed and installed onboard.

The DP controller developed for the case study has been designed in order two be able to deal with different manoeuvres. In particular, two different types of control modes have been developed: the (open-loop) joystick mode and the (closed-loop) station-keeping control and their structures are presented herein.

Author's Biography

Michele Martelli was born in Italy in 1985. He received the B.S., M.S., and PhD degrees in marine engineering and naval in 2006, 2009, and 2013, respectively. Currently, he is Associate Professor at the University of Genova. He is a co-author of more than 50 scientific papers. His main research interest focuses on the study of the dynamics of the propulsion plant and its control system. Since 2010, he has been actively working on several research projects, funded by both private and public companies.

Nicolò Faggioni was born in Italy in 1991. He received his Bachelor's degree in Nautical Engineering in 2014 and the Master's degree in Yacht Design in 2017 from the University of Genoa. Currently, he is PhD student in Naval Architecture and Marine Engineering, started in November 2018, at DITEN of Genoa University. His main research interests concern ship propulsion plants, mathematical models and numerical simulation.

Silvia Donnarumma received the Ph.D. degree in Mathematical Engineering and Simulation from the University of Genoa, Genoa, Italy, in 2016. Her research interests include the study and application of nonlinear control techniques, based on hybrid approaches (with resets) and on convex optimization techniques based on LMIs, for the synthesis of feedback control systems; dynamic positioning system; control with actuator saturation, and automatic steering in general.

 https://doi.org/10.24868/issn.2631-8741.2020.002

Hence, the paper aims to highlight the differences between DPCPs obtained with both the static and dynamical approaches. Moreover, results are obtained with the same environmental mathematical models in order to evaluate the influences of the dynamical effect of disturbances. A more detailed description of the model characteristics and the used mathematical models are reported in Section 2, while the thrust allocation logic and the controller structure is shown in Section 3. The results of the simulation campaign for both controller modes are reported in Section 4. Eventually, the conclusion and recommendations are shown in Section 5.

2. Simulation Platform

2.1. Case study

The testing case is a tugboat model with an overall length (Loa) of 0.97 m and a maximum width of 0.30 m. The model is composed of: (i) *two azimuth thrusters*, one for each shaft-line equipped with a ducted propeller, the Z-layout mechanical transmission with two coupled bevel gears; (ii) *two electric motors*, DC motors and a specific DC drive; (iii) *one bow-thruster*, driven by an electric motor, controlled by its DC drive.

The new control logics will be implemented on the testing model shown in Figure 1.

Figure 1: Testing Model

2.2. Dynamic ship simulator model

The developed simulator accounts for 3 degrees of freedom (DOF), surge, sway, and yaw. The reference frames used in the analysis are shown in the following figure.

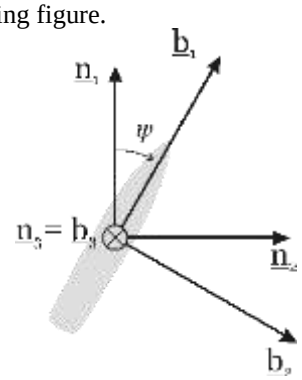

Figure 2: Reference frames

A 3 DOF model is supposed to be enough for the design and the evaluation of the performance of the actuators. Moreover, for the actual model configuration is not possible to counteract forces and moments in the vertical plane, Sørensen (2011). Moreover, the effect of the waves drift forces in the horizontal plane could be taken into account by using a simplified methodology (for instance using DNV-GL rules), this aspect is relevant in evaluating the station keeping performances. For such a reason, further investigations will be carried out in future. Albeit, in the presented application, the focus was on the optimisation of the thrust allocation, and this is independent of the magnitude of the external disturbances.

The vessel dynamics are evaluated by considering the ship as a rigid body and assuming a constant displacement. Under the previous assumptions, it is possible to obtain the ship acceleration, velocity, and position by using IInd Newton's law. The ship's quasi-velocity components (u, v, r) in the ship fixed frame $(\underline{b}_1, \underline{b}_2, \underline{b}_3)$ and the ship's displacements in the earth inertial frame (x, y, ψ), can be assessed by using the following equation:

 https://doi.org/10.24868/issn.2631-8741.2020.002

$$\begin{cases} M(\dot{u} - x_G r^2 - uv) = X_h + X_p + X_e + X_c \\ M(\dot{v} + x_G \dot{r} + ur) = Y_h + Y_p + Y_e + Y_b + Y_c \\ I_{zz}\dot{r} + M x_G(\dot{v} + ru) = N_h + N_p + N_e + N_b + N_c \end{cases} \quad (1)$$

where: h, p, e, b, c subscripts refer to the hull, the propellers, the environmental disturbances, the bow-thruster, and Coriolis, respectively; M is the sum of ship's mass and added mass; I_{zz} is the ship inertia concerning $\underline{b_3}$. x_G is the longitudinal position of the centre of gravity.

The simulator is composed of subsets of mathematical equations, each one reproducing a specific sub-system of the vessel: (i) *propulsion plant*, DC electric motor models, shaft lines and, thrusters; (ii) *bow-thruster*, DC electric motor, transmission and propeller models; (iii) *hull forces*, hull forces and moment at low-speed for high drift angles (Oltmann & Sharma, 1984); (iv) *environmental forces*, disturbances effect on the vessel. The DNV-GL formulation (2016), was used to assess the wind forces. In the following, a brief description of the mathematical models used is reported.

2.2.1. Propulsion plant

As already introduced, the propulsion system model is composed of 3 subsets: DC electric motor, shaft line, and propeller. The DC electric motor behaviour is described by the electromechanical differential equation, as follows:

$$\frac{di}{dt} = -\frac{R}{L} i(t) - \frac{1}{L} K_e n_e(t) + \frac{1}{L} V_{app}(t) \quad (2)$$

where: $i(t)$ is the current intensity, R is the resistance, L is the inductance, the K_e is an electric constant related to the electrical wiring system, $n_e(t)$ is the motor speed and, V_{app} is the applied voltage. The DC delivered torque, $Q_{DC}(t)$, is proportional to an electric motor constant and the current induced by the applied voltage.

$$Q_{DC}(t) = K_e\, i(t) \quad (3)$$

The selection of this model is considered a good compromise between the small number of parameters to identify and a reliable reproduction of the dominant dynamics. The differential equation representing shaft-line behaviour is reported hereinafter:

$$I_T\, \dot{n}_e = \sum Q(t) = Q_{DC}(t) - Q_{fric}(t) - Q_P(t) \quad (4)$$

where: I_T is the sum of all inertia elements, $\dot{n}_e$ is the motor angular acceleration, $Q_{DC}(t)$ is delivered torque, $Q_{fric}(t)$ is the friction torque; and $Q_P(t)$ is the required propeller torque. In particular, the friction torque, $Q_{fric}(t)$ is obtained by the following relation:

$$Q_{fric}(t) = Q_{DC}(t)\,(1 - \eta_{TR}(n_e)) \quad (5)$$

where: η_{TR} is the transmission efficiency, depending on the engine speed, n_e; $\eta_{TR} \in [0.65, 0.98]$ with lower and upper bounds corresponding to idle condition and maximum engine speed, respectively; η_{TR} trend is logarithmic as described in Martelli et al. (2019) The required propeller torque, $Q_P(t)$, is described by the following relation:

$$Q_P(t) = \frac{Q_O(t)}{\eta_R} \quad (6)$$

where: Q_O, is the required open water torque and η_R, is a relative rotative efficiency, and it is assumed to be constant. The propeller geometry of the test model is consistent with the Wageningen 19A propeller (Kuiper, 1992). The delivered thrust and required torque are evaluated by using $C_T(\beta)$ and $C_Q\,(\beta)$ coefficients in the four-quadrant notation. A quasi-dynamic method is adopted to evaluate the propeller force in the time domain. All the quantities depend on the advance angle, β:

$$\beta = \tan^{-1}\frac{J}{0.7\,\pi}\;;\; J = \frac{V_A}{n_p D}\;;\; V_A = V(1-w) \quad (7)$$

$$V_r = \sqrt{{V_A}^2 + (0.7\,\pi\, n_p\, D)^2} \quad (8)$$

$$T_O = \tfrac{1}{2}\rho\,\tfrac{\pi D^2}{4}\,V_r^2\,C_T\;;\; Q_O = \tfrac{1}{2}\rho\,\tfrac{\pi D^3}{4}\,V_r^2\,C_Q \quad (9)$$

where: J is advance coefficient, V_A is the advance speed, n_p is the propeller speed, D is the propeller diameter, V is the vessel speed, w is the wave factor, V_r is the relative speed, ρ is the water density, T_O is the open water thrust, and Q_O is the open water torque. Hence, the forces and moment expressed in the ship fixed frame are defined as:

$$\begin{cases} X_p = T_O \cos\delta \\ Y_p = T_O \,\mathrm{sen}\,\delta \\ N_p = Y_p x_p - X_p y_p \end{cases} \quad (10)$$

 https://doi.org/10.24868/issn.2631-8741.2020.002

where: δ is the geometric azimuthal angle, x_p and y_p represent the coordinates of the propeller with regard to the ship fixed frame.

2.2.2. Bow thruster

The bow-thruster has been modelled as a ducted propeller. It is possible to evaluate the delivered thrust (T_{Ob}) and the required torque (Q_{Ob}) through $K_T(J)$ and $K_Q(J)$ coefficients belonging to the tunnel thrusters of the Wageningen series, as described in the following:

$$T_{Ob} = \rho K_T(J)\, {n_p}^2 D^4 \; ; \; Q_{Ob} = \rho K_Q(J)\, {n_p}^2 D^5 \tag{11}$$

where V_A is the advance velocity which is evaluated as follows:

$$V_A = v + r\, x_{BT} \tag{12}$$

where: v is the velocity component along the y-axis, and x_{BT} is the distance between the bow-thruster tunnel and the origin of the ship-fixed reference frame. Hence:

$$\begin{cases} X_b = 0 \\ Y_b = T_{Ob} \\ N_b = Y_p x_{bt} \end{cases} \tag{13}$$

2.2.3. Hull Forces

The hull forces are evaluated by using Oltmann & Sharma approach. The proposed model provides a realistic representation of the hydrodynamic force performance for low-speed manoeuvres at high drift angle. Then, according to Oltmann & Sharma (1984), the total hydrodynamic force is composed by three main contributions: ideal fluid forces (I), lift forces (HL), and cross-flow drag forces (HC), the formulation for 3-DOF is the following:

$$\begin{cases} X_h = X_I + X_{HL} - R_T \\ Y_h = Y_I + Y_{HL} + Y_{HC} \\ N_h = N_I + N_{HL} + N_{HC} \end{cases} \tag{14}$$

where: X_i refers to the force along $\underline{b}_1$, Y_i refers to the force along $\underline{b}_2$, and, N_i refers to the moment around $\underline{b}_3$.

The contribution of the hull resistance, R_T, in explicitly considered as a separate term. The ideal fluid forces (I) are assessed through the following considerations: by using the potential theory (neglecting the effects of viscosity), the hydrodynamic forces, generated by a body that moves in an ideal, irrotational fluid that does not generate lift, can be expressed through a mass matrix and added inertia depending exclusively on the body shape. The wavefield formation phenomenon can be ignored (simplification acceptable for low Froude numbers considered).

Lift forces (HL) can be assessed through the following considerations: a body in a fluid that moves at a given speed with a certain angle of attack generates lift forces equivalent to a wing profile. The hull can be seen as a low aspect ratio wing. A lift force, orthogonal to the flow, F_L, and an induced resistance parallel to it, F_D, are therefore generated. These forces are mainly dependent on the drift angle, β, which represents the angle of attack of the profile.

Cross-Flow Drag (HC) forces represent the contribution of resistance due to the viscous forces generated by a moving body in a real fluid. Such term considers the hull divided into mutually non-influential sections and analyses each section of length dx placed at a distance x from the origin of the axes.

2.2.4. Environmental Forces

The environmental forces have been evaluated under the hypothesis of the linear superposition principle:

$$\begin{cases} X_e = X_w + X_c + X_{wind} \\ Y_e = Y_w + Y_c + Y_{wind} \\ N_e = N_w + N_c + N_{wind} \end{cases} \tag{15}$$

where $w, c, wind$ subscripts refer to wave, current, and wind, respectively.

In the proposed simulations, only the wind action is taken into account, because, at the current state of research, it is not possible to validate the current and wave actions due to limitations in the experimental benchmark. The DNV-GL rules provide the formulation for all disturbance model actions. For the sake of shortness, hereinafter only the wind formulation is reported:

 https://doi.org/10.24868/issn.2631-8741.2020.002

$$\begin{cases} X_{wind} = \frac{1}{2}\rho_{air}{V_{wind}}^2 A_{F,wind}(-0.7\cos(\gamma_{rel})) \\ Y_{wind} = \frac{1}{2}\rho_{air}{V_{wind}}^2 A_{L,wind}(0.9\sin(\gamma_{rel})) \\ N_{wind} = Y_{wind}\left(x_{L,air} + 0.3\left(1 - 2\frac{\gamma_{rel}^i}{\pi}\right)L_{pp}\right) \end{cases} \quad (16)$$

$$\gamma_{rel}^i = \begin{cases} \gamma_{rel}, & 0 \le \gamma_{rel} \le \pi \\ 2\pi - \gamma_{rel}, & \pi \le \gamma_{rel} \le 2\pi \end{cases}$$

where: ρ_{air} is the air density, V_{wind} is the wind speed, $A_{F,wind}$ is the frontal projected wind area, $A_{L,wind}$ is the longitudinal projected wind area, $x_{L,air}$ is the longitudinal position of the lateral projected area centre (in the body-fixed frame), and γ_{rel} is the relative wind direction.

The proposed relations are suitable for both static and dynamic simulations. In particular, in the dynamic analysis, the relative wind direction is supplied by the instantaneous encounter angle. Besides, the wind speed is considered through the Davenport spectrum model tailored in order to generate allowable wind gust for the proposed model test. Namely, the maximum deviation from the average set value is 5%. The wind speed V_{wind}, implemented in the simulator is evaluated by means the following formulation:

$${V_{wind}}^2 = (V_{m,wind} + v_{g,wind})^2 \cong {V_{m,wind}}^2 + 2V_{m,wind}v_{g,wind} \quad (17)$$

where: $V_{m,wind}$ is the average wind speed, and $v_{g,wind}$ is the wind gust speed.

3. Dynamic positioning system

3.1. Controller structure

The controller structure is based on the one proposed by Alessandri et al. (2019) which provides an integrated structure for motion control. In this application, the motion controller orchestra realises on an optimised force allocation logic, and the input belongs switching between open and closed loop controllers. In particular, forces and moment requirements can be alternatively the output of the joystick or the motion controller, as sketched in Figure 3. The joystick output is independent requirements of force and moment, as well as controller output, are forces and moment necessary to compensate for the action of environmental disturbances by means of position and speed errors. For the sake of compactness, quantities are presented in matrix form. In particular, the array $\tau_i = [X_i, Y_i, N_i] \in \Re^n$ contains forces components along $\underline{b}_1$, $\underline{b}_2$ and the moment around $\underline{b}_3$, respectively. The subscripts R and D indicate the requested and delivered quantities. In the following all the forces, moment, and thrusts are referred to superscript $*$ that represents that quantities are divided by the maximum allowable thrust of the azimuthal propeller. Then, by using the general structure the requested forces and moment τ_R^* are defined hereinafter, the first set is referred to the joystick mode, while in the second one is related to the DP.

$$\tau_R^* = \begin{cases} X_{joystick}^* \\ Y_{joystick}^* \\ N_{joystick}^* \end{cases} \quad \text{or} \quad \tau_R^* = \begin{cases} K_{P_x}e_x^* + K_{D_x}e_{\dot{x}}^* + K_{I_x}\int e_x^* - K_{AW_x}(X_R^* - X_D^*)d\zeta \\ K_{P_y}e_y^* + K_{D_y}e_{\dot{y}}^* + K_{I_y}\int e_y^* - K_{AW_y}(Y_R^* - Y_D^*)d\zeta \\ K_{P_\psi}e_\psi^* + K_{D_\psi}e_{\dot{\psi}}^* + K_{I_\psi}\int e_\psi^* - K_{AW_\psi}(N_R^* - N_D^*)d\zeta \end{cases} \quad (18)$$

where: $X_{joystick}^*, Y_{joystick}^*, N_{joystick}^*$ are the non-dimensional forces corresponding to joystick lever positions, $[K_{P_x}, K_{P_y}, K_{P_\psi}]$ $[K_{D_x}, K_{D_y}, K_{D_\psi}]$, $[K_{I_x}, K_{I_y}, K_{I_\psi}]$, and $[K_{AW_x}, K_{AW_y}, K_{AW_\psi}]$ are proportional, derivative, integral, anti-windup controller coefficients, respectively. Indeed, in order to accurately assess the DP controller, an anti-windup component is added in order to limit *windup integral* divergences (Alessandri et al. 2014). In Figure 3, a simulation platform block model is sketched with attention to the switching mode. Indeed, as previously illustrated, the joystick and DP controller output are required forces and moment that are necessary to follow a user-defined direction or to keep the required position. Then, a unique force allocation logic can accomplish with both the requirements.

 https://doi.org/10.24868/issn.2631-8741.2020.002

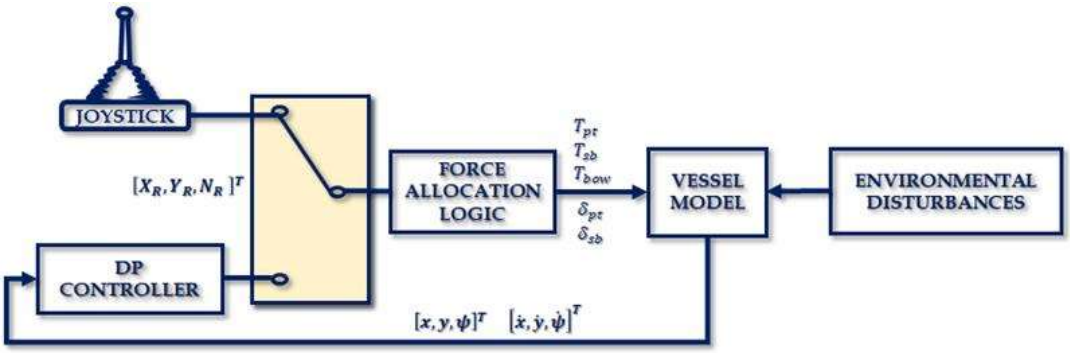

Figure 3: Controller structure.

3.2. The Thrust Allocation Logic

In this section, the allocation logic implemented in order to assess both joystick manoeuvre and dynamic positioning capabilities is illustrated. The logic is based on a constrained optimisation problem that makes the use of the Lagrange multiplier method able to minimise an objective function under opportune constraints. In particular, the domain of the function is $\underline{x} = \left[T_{pt}^*, T_{sb}^*, T_{bow}^*, X_{pt}^*, Y_{pt}^*, X_{sb}^*, Y_{sb}^*\right] \in \mathbb{R}^7$ where $\underline{T}_{pt}^* = X_{pt}^* \underline{b}_1 + Y_{pt}^* \underline{b}_2$ is the vector of portside thrust, $\underline{T}_{sb}^* = X_{sb}^* \underline{b}_1 + Y_{sb}^* \underline{b}_2$ is the vector of starboard thrust and $\underline{T}_{bow}^* = Y_{bow}^* \underline{b}_2$ is the vector of the bow-thruster thrust. The problem is formulated as it follows:

$$\min_{\underline{x}} f(\underline{x}) \quad \text{with} \quad h_i(\underline{x}) = 0 \quad \text{and} \quad g_j(\underline{x}) > 0 \tag{19}$$

where $f(\underline{x})$ is the objective function $f(\underline{x}): \mathbb{R}^n \longrightarrow \mathbb{R}$

$$f(\underline{x}) = \left(\frac{T_{pt}^*}{T_{max}^{tot}}\right)^2 + \left(\frac{T_{sb}^*}{T_{max}^{tot}}\right)^2 + \left(\frac{T_{bow}^*}{T_{max}^{tot}}\right)^2 \tag{20}$$

The constraints $h_i(\underline{x}): \mathbb{R}^n \longrightarrow \mathbb{R}^m$ are the following

$$\begin{cases} h_1(\underline{x}) = X_R^* - X_{pt}^* - X_{sb}^* \\ h_2(\underline{x}) = Y_R^* - Y_{pt}^* - Y_{sb}^* - T_{bow}^* \\ h_3(\underline{x}) = N_R^* - x_{bow}\ T_{bow}^* - x_{pt}\ Y_{pt}^* + + y_{pt}\ X_{pt}^* - x_{sb}\ Y_{sb}^* + y_{sb}\ X_{sb}^* \\ h_4(\underline{x}) = T_{pt}^{*2} - X_{pt}^{*2} - Y_{pt}^{*2} \\ h_5(\underline{x}) = T_{sb}^{*2} - X_{sb}^{*2} - Y_{sb}^{*2} \end{cases} \tag{21}$$

where: $[X_R^*, Y_R^*, N_R^*]$ are the required forces and moment. Such components are the output of the controller when the automatic motion control is active, and the loop is closed and the joystick output in open loop mode when the lever is active. The following constraints are added in order to guarantee that the relationship between the vector components and their moduli.

$$g_1(\underline{x}) = T_{pt}^* \quad , \quad g_2(\underline{x}) = T_{sb}^* \tag{22}$$

4. Simulation Results

4.1. Joystick mode results

As described in Section 3, two modes are user-selectable: the joystick mode (open-loop) and DP (closed-loop). The performances of the joystick mode are evaluated by simulation, and the results are described in the following. In this manoeuvre, the user commands the ship to act first a pure crabbing motion starting from zero speed, then a pure forward motion, and eventually a pure rotation on the spot.

Figure 4 shows the time history of the joypad signal input; a three-axis controller is sufficient to control high drift angle manoeuvres. In this first installation, three independent controllers were used, one for each axis as for the DP. In the reported manoeuvre, the operator requires a pure crabbing (blue line) to portside for the first 15 s. After that, the user, before moving to pure surge (red dashed line) slows the drift speed down in order to bring the initial conditions as close to the original as possible. Then, pure yaw on the spot has been selected as drawn by the cyan dashed line.

 https://doi.org/10.24868/issn.2631-8741.2020.002

In Figure 5, the required (blue lines) and the delivered (red dotted lines) forces and moment related to the actuators are shown. As can be seen, all the requirements are met by the vessel. Such a result efforts the chosen allocation logic with respect to the required forces setpoint. The forces are presented in dimensionless form, with respect to the maximum thrust of one propeller. Similarly, the moment has been presented in dimensionless form dividing by the maximum delivered moment of one propulsor.

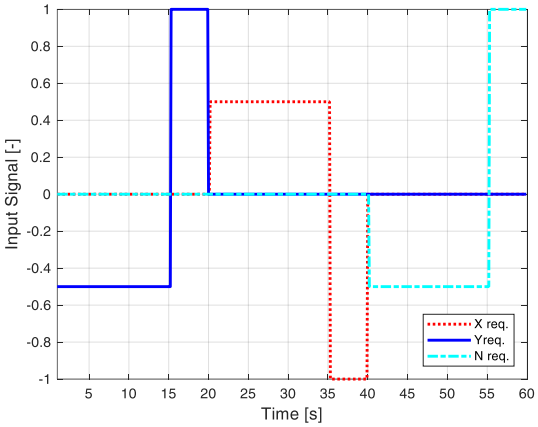

Figure 4: Joypad Output Signal

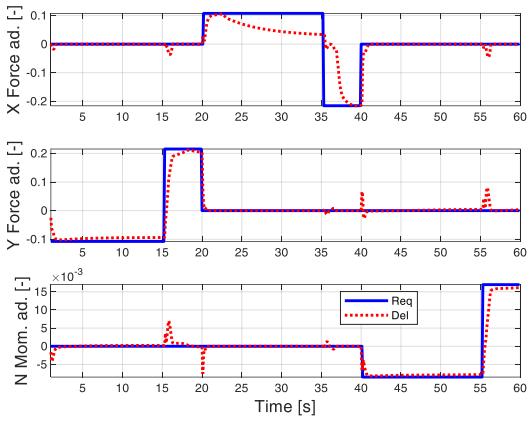

Figure 5: Actuated and Requested Forces and Mom.

In Figure 6, the comparison between required (blue line) and actuated (red dotted line) azimuth angles are shown.

In Figure 7, the dimensionless path is reported (light blue line); initial and final conditions are shown with dashed green and continuous red waterlines, respectively; and waterline time history with a blue line. It can be seen that the commands are well performed with the minimum amount of delivered thrust. During the last part of the manoeuvre, the pure yaw the boat has almost rotate anticlockwise for 180°.

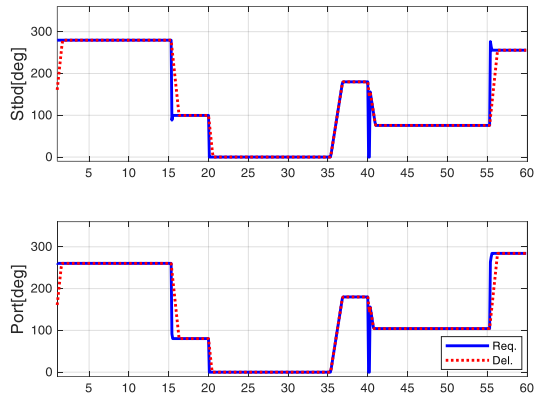

Figure 6: Actuated and Requested Azimuth Position

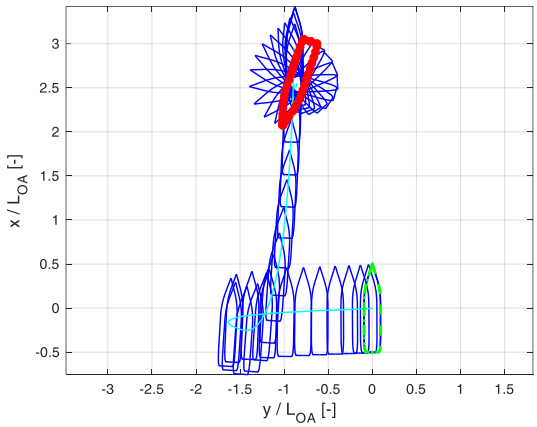

Figure 7: Dimensionless Path

4.2. Dynamic positioning - Dynamic and static DP capability plot

In this section, station-keeping dynamic results are presented. The main idea is to compare DPCPs obtained by static approaches and those obtained by simulations. The main expected differences concern two main factors: (i) the influence of transients, which do not have a great impact on the assessment of DP performance, but which can affect performance during changes in environmental conditions in operations; (ii) disturbance fluctuations, such as the effect of wind gusts, which can increase the average value by several percentage points. Indeed, DP performances are usually estimated through the DP capability polar plots with particular attention to the reliability of environmental disturbances. Moreover, the interaction between the external disturbances and the vessel involves dynamics that are not taken into account with the static approach. For such a reason, the developed simulation platform is used to obtain the DP capability plot by dynamic assessment results. In particular, 180 simulations have been conducted with different wind speed (from 6 to 15 kn with 1 kn step) and several incoming directions

 https://doi.org/10.24868/issn.2631-8741.2020.002

(from 0° to 180° with a step of 10°). The duration of each simulation was set to 600 s, and maximum allowable errors are 0.7 L_{OA} from the desired position and ± 15° from the desired bow angle.

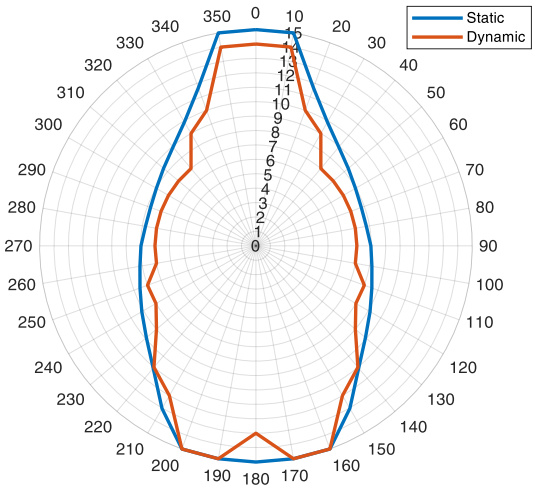

Figure 8: Comparison between static and "dynamic" DP capability plot

Figure 8 shows the difference between a standard DP capability polar plot (blue line) and the one obtained with the dynamic analysis (orange line). The more significant differences are experienced for wind coming from the bow quartering wind and stern direction. Such results enhance what was expected. In particular, there are no significant differences in the station keeping capability of the vehicle. On the other hand, the influence of the disturbances dynamics together with the differences in the actuator time responses impose considerations to be made on the extreme values obtained with the static approach. Indeed, in the static analysis, the equilibrium was evaluated with a fixed encounter angle, fixed wind speed, and without taking into account for the actuators rate limiters. For these reasons, tolerance constraints have been considered in the simulations. In order to emphasise the additional information obtained by using a simulation-based design approach, the time histories, of some significant quantities evaluated during a simulation with wind mean speed of 8 kn and incoming direction of 160° are shown in dimensionless form over their maximum values.

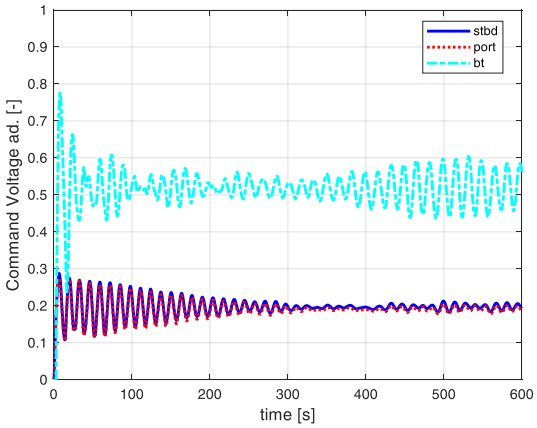

Figure 9: Required Voltage 160° 8kn

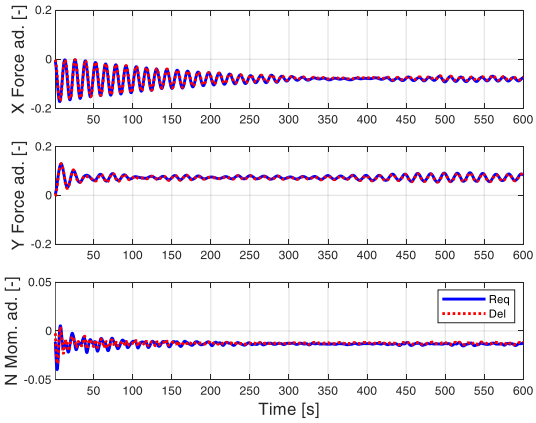

Figure 10: Actuated and Required Forces and Moment 160° 8kn

In Figure 9, the required engine voltages time histories are presented. In Figure 10, forces and moment required by the controller in order to compensate disturbance action (evaluated by means of positional errors) are compared with the delivered ones.

 https://doi.org/10.24868/issn.2631-8741.2020.002

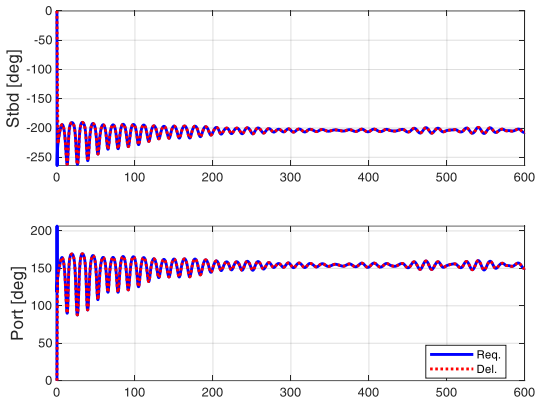

Figure 11: Actuated and Required Azimuth Position 160° 8kn

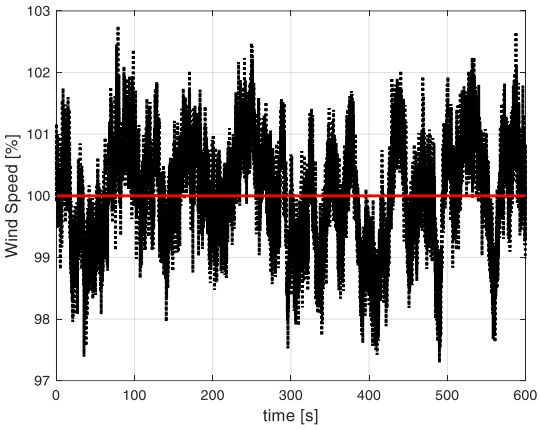

Figure 12: % Wind Speed 160° 8kn

Figure 11 reports the time history of the required and delivered azimuth angles. In Figure 12, the time history of percentage variation of wind speed (black line) is reported, the mean wind speed, equal to 8 kn, is the red line.

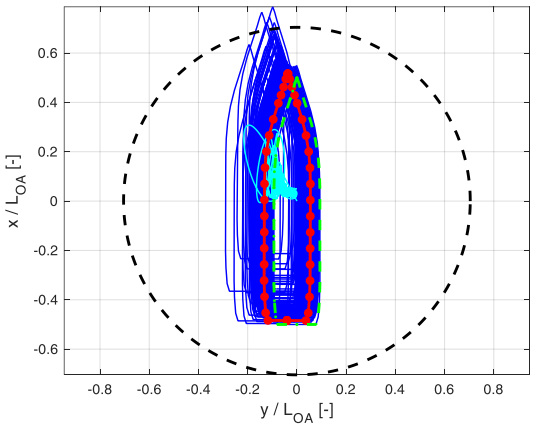

Figure 13: Dimensionless Path 160° 8kn

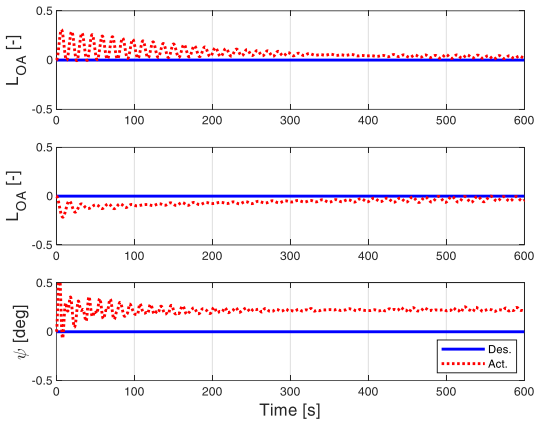

Figure 14: Displacements 160° 8kn

In Figure 13, the path of the vessel is reported with a cyan line. As can be seen, midship never overtakes the black dashed circle line, which represents the maximum allowable error. Eventually, in Figure 14, the displacements for x and y-axes (over the ship length) and rotation on z-axis are reported.

5. Conclusions & recommendations

The presented paper aims to show a new approach to evaluate the dynamic positioning capability of a vessel. Moreover, the importance to conduct a DP dynamic analysis is highlighted whenever the system performance in a realistic environment needs to be evaluated. The authors consider that the static approach is still valid for the design of the main characteristics of the propulsion system and for a first analysis of its performance. On the other hand, it is not possible to understand, from the static results, if the vehicle will be able to overcome the transient safely nor if the vehicle can withstand, even small, oscillations around the equilibrium reached configuration. The presented DP system has been developed with an optimised thrust allocation that can be used in both open-loop joystick mode and in closed-loop dynamic positioning mode; both modes were successfully tested. Besides, the paper encourages the designers to analyse the DP system with a dynamic approach; in fact, sometimes significant differences are experienced compared to the static approach results. By using a dynamic approach it is possible to evaluate the transients of manoeuvring and also analyse how the DP control logic responds in the function of the different magnitude of disturbances. This information is not available with other design methods. The future development will regard the implementation of the thrust allocation on the hardware testing model, and the analysis of the experimental manoeuvring behaviour concerning the numerical results.

 https://doi.org/10.24868/issn.2631-8741.2020.002

References

Alessandri, A., Donnarumma, S., Luria, G., Martelli, M., Vignolo, S., Chiti, R., & Sebastiani, L. (2014). Dynamic positioning system of a vessel with conventional propulsion configuration: Modeling and simulation. In *Proc. Martech 2nd Int. Conf. Maritime Technol. Eng.* (pp. 725-733), Lisbon, Portugal.

Alessandri, A.; Donnarumma, S.; Martelli, M.; Vignolo, S. (2019). Motion Control for Autonomous Navigation in Blue and Narrow Waters Using Switched Controllers. J. Mar. Sci. Eng. 2019, 7, 196.

Assessment of station keeping capability of dynamic positioning vessels (2016). Standard — DNVGL-ST-0111. Edition July 2016.

Donnarumma, S., Martelli, M., & Vignolo, S. (2015). Numerical models for ship dynamic positioning. In 6th International Conference on Computational Methods in Marine Engineering, MARINE (pp. 15-17).

Donnarumma, S., Figari, M., Martelli, M., Vignolo, S., & Viviani, M. (2017). Design and validation of dynamic positioning for marine systems: A case study. IEEE Journal of Oceanic Engineering, 43(3), 677-688.

Johansen, T.A. & Fossen, T.I. (2013). Control allocation—A survey. In Automatica, 49(5), 1087-1103, https://doi.org/10.1016/j.automatica.2013.01.035.Kuiper, G. (1992). The Wageningen propeller series (No. BOOK). Marin.

Martelli, M., Faggioni, N., & Berselli, G. (2019). Fuel saving in a marine propulsion plant by using a continuously variable transmission. Proceedings of the Institution of Mechanical Engineers, Part M: Journal of Engineering for the Maritime Environment, 233(4), 1007-1021.

Oltman, P. & Sharma, S.D. (1984). Simulation of Combined Engine and Rudder Maneuvers using an improved Model of Hull-Propeller-rudder Interactions, Proc. 15thONR, pp.83-108.

Reilly, G. T., & Hensley, M. (2011). Dynamic Positioning Capability and Enhanced Reliability. Offshore Technology Conference, OTC Brasil, 4-6 October, Rio de Janeiro, Brazil.

Sørensen, AJ (2011). A survey of dynamic positioning control systems. In Annual Reviews in Control, 35(1), 123-136, https://doi.org/10.1016/j.arcontrol.2011.03.008.

Sørensen, A. J., Sagatun, S. I., & Fossen, T. I. (1996). Design of a dynamic positioning system using model-based control. Control Engineering Practice, 4(3), 359-368.

Xu, S., Wang, X., Wang, L., Meng, S., & Li, B. (2015). A thrust sensitivity analysis based on a synthesised positioning capability criterion in DPCap/DynCap analysis for marine vessels. *Ocean Engineering*, *108*, 164-172. Wang, L., Yang, J. & Xu, S. (2018). Dynamic Positioning Capability Analysis for Marine Vessels Based on A DPCap Polar Plot Program. China Ocean Eng 32, 90–98. https://doi.org/10.1007/s13344-018-0010-4.

 https://doi.org/10.24868/issn.2631-8741.2020.002